XUE-SHI LI | Researcher
Guangdong University of Technology, Guangzhou, PRC

KAI-DA XU | Researcher
EHF Key Lab of Fundamental Science, University of Electronics Science and Technology of China, Chengdu, PRC

ZHI-MIN LIU | Researcher
Guangdong University of Technology, Guangzhou, PRC

DONG-YUE ZHOU | Researcher

FEI DU | Researcher

METAMATERIAL Extends Patch Antenna Bandwidth

By leveraging a reactive impedance surface (RIS) metamaterial, this patch antenna design covers a wide bandwidth with high gain, serving a number of different wireless applications.

Patch antennas serve many different wireless applications, both for voice and data communications. When based on a metamaterial with reactive impedance surface (RIS), these antennas can achieve extended bandwidths of 1.70 to 5.26 GHz, and even more. By using an RIS metamaterial, a patch antenna with that bandwidth and peak gain of 7.24 dB was fabricated, with excellent radiation characteristics.

The antenna features a single structure of a one-layer substrate. It boasts a compact footprint that is only $0.408\lambda_0 \times 0.357\lambda_0$ at the lowest operating frequency (1.70 GHz). The antenna's wide bandwidth makes it well suited for a wide range of applications, including Bluetooth (2400 to 2480 MHz), Wibro (2300 to 2390 MHz), and WiMAX (3300 to 3700 MHz).

Metamaterials are essentially materials that began in the laboratory, rather than in nature. They are engineered to provide material characteristics that cannot be found in nature. Metamaterials include composite formulations of materials with improved electromagnetic (EM) or photonic characteristics or improved mechanical traits, such as enhanced flexibility.

Metamaterials can support a wide range of applications, and have been used as building blocks in antenna designs, as microwave absorbers, and even to counteract the effects of seismic waves during earthquakes, as a form of seismic material protection. The behavioral patterns of different types of metamaterials have been simulated on computers by means of three-dimensional (3D) models and with the aid of modern computer-aided-engineering (CAE) software programs, and the availability of these advanced EM metamaterials offers RF/microwave engineers a new frontier for the design of some traditional passive components, such as antennas, and the wideband patch antenna described herein.

Patch antennas based on metamaterials offer many benefits, including wide bandwidths, miniaturization, and well-controlled radiation characteristics. Because of their many benefits, metamaterial antennas have been used for many applications, including the aforementioned Bluetooth, Wibro, and WiMAX, as well as WCDMA operating from 1920 to 2170 MHz.[1,2] Still, improvements need to be made to these antennas, which typically involve complex structures with low gain as tradeoffs for the wide bandwidths.

To improve metamaterial antenna performance levels, novel metamaterial structures like multiple split ring resonators (MSRRs), reactive impedance surface (RIS) designs, partial reflective surface (PRS) designs, and mushroom-like electromagnetic bandgap (EBG) structures have been developed in recent years.[3-7] The composite-split-ring-resonator (CSRR) structures etched on the patch along with the substrate, and the ground plane can be optimized for miniaturization.[8]

To change an antenna from linear to circular polarization, the chiral patterned metamaterial placed over the radiation patch of an antenna was proposed.[9] The RIS has a simple pattern that is composed of periodic metallic patches. It is good for expanding the operating bandwidth and enhancing the radiation gain.[10,11] In recently published reports on metamaterial antennas, an RIS-like pattern was etched on the ground with a one-layer substrate, and metamaterial inspired structures were being etched on the patch.[12-14]

This type of metamaterial antenna is a good example of extending the bandwidth while keeping the radiation performance attractive. It could be made even more valuable using a simpler structure while maintaining the relatively high operating frequencies (above 3 GHz). This is helpful for portable applications at lower frequencies, such as WCDMA, Bluetooth, or Wibro.

From a practical point of view, it might be desirable to simplify the antenna structure for ease of fabrication while shifting the operating frequency of the antenna in ref. 12 to a lower band. To meet these requirements, a one-layer patch antenna was developed based on the RIS metamaterial approach. The RIS structure is formed by means of an etched ground as well as the patch.

The metamaterial-inspired antenna employs simple structures since there is only one substrate layer and an intact patch applied in the antenna. The antenna achieves a wide operating frequency band at the lower frequencies. It is attractive for multiple-band applications, including WCDMA, WiMAX, Bluetooth, and Wibro.

To achieve broadband coverage with a simple structure, an antenna was developed using RIS metamaterial. The antenna configuration is based on a one-layer patch design. It was constructed by etching strip gaps on the ground while leaving the patch intact, thus forming a RIS structure. The antenna is excited by a microstrip line that connects the patch and the input port.

The RIS metamaterial is employed to broaden the operating frequencies and enhance the radiation performance of the antenna via its reactive coupling with the patch and substrate. The antenna's performance was simulated by the electromagnetic (EM) High-Frequency Structure Simulator (HFSS) software from Ansoft (www.ansoft.com), and the simulations yielded results that were quite in keeping with the measured performance of the fabricated antenna.

Figure 1 shows the structure of the antenna. To extend the operating bandwidth, the RIS is formed by the patch and the strip-gap etched ground. It is used to enhance the radiation performance as well as broaden the bandwidth of the antenna. It should be noted that there are some distinct differences between the antenna presented here and the antenna in ref. 12. The slots etched onto the patch

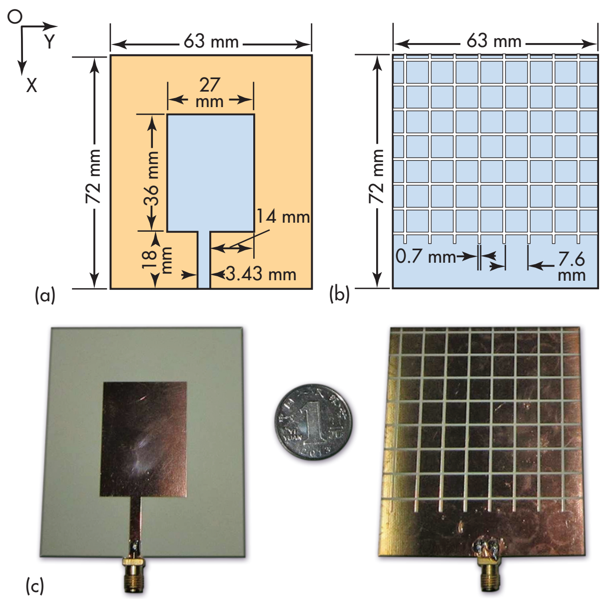

1. The diagrams show (a) the top view and (b) bottom view of the antenna, along with (c) the fabricated antenna.

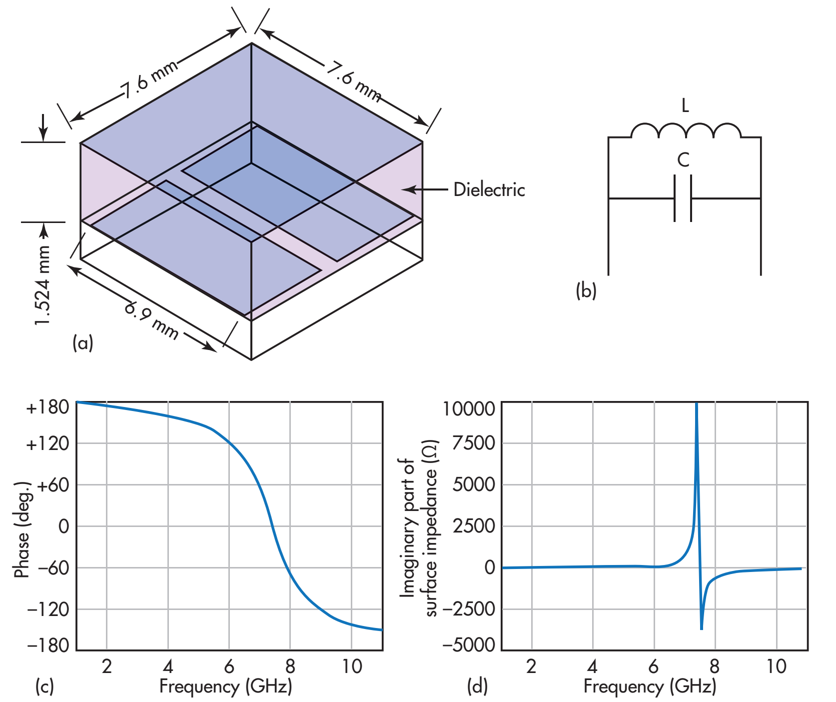

2. The diagram shows (a) a unit cell next to (b) a simple circuit model, (c) a phase response, and (d) a plot of the imaginary surface impedance.

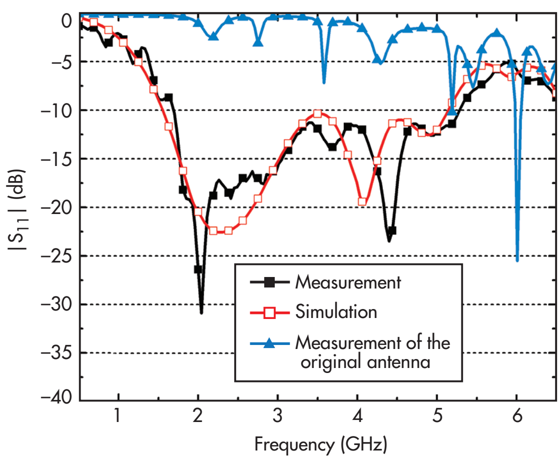

3. These plots show measured and simulated reflection coefficients for the antenna.

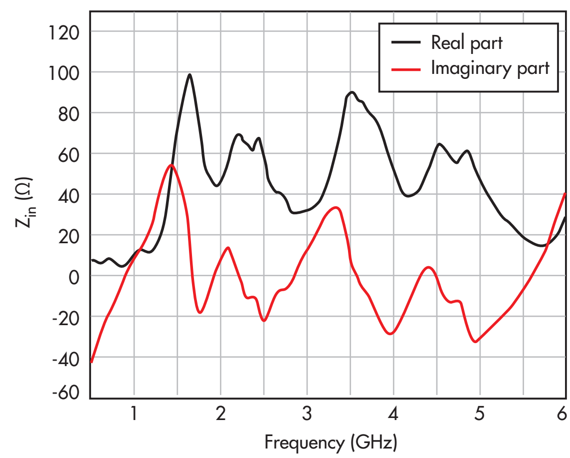

4. These curves show the real and imaginary measured input impedance responses for the antenna.

of the antenna in ref. 12 have been eliminated while maintaining favorable performance. By using an intact patch, the structure of the antenna is further simplified, for ease of fabrication. In addition, the operating band is shifted towards lower frequencies than the design of ref. 12 (above 5.3 GHz) to cover the frequency bands of WiMAX, WCDMA, Bluetooth, and Wibro.

Figure 1(c) shows the fabricated antenna. It is formed on RO4350B printed-circuit-board (PCB) material from Rogers Corp. (www.rogerscorp.com) with a relative dielectric constant, $\varepsilon_r = 3.66$ in the z-axis (thickness) at 10 GHz. The thickness (h) of the substrate was fixed to be as small as 1.524 mm. The overall antenna footprint was only $0.408\lambda_0 \times 0.357\lambda_0$ at the lowest operating frequency of 1.7 GHz.

The strip-gap etched ground together with the antenna patch above it can be considered a type of metamaterial—namely, RIS. To analysis the influence of the RIS on the performance of the antenna, one unit cell of the RIS was built up and then the periodic boundary condition is applied on the four lateral walls of the unit cell. In this way, an infinite array of the unit cell forming the RIS structure is constructed for analysis. The dimension of the unit cell is the same as the RIS structure employed in the antenna of *Fig. 2*. The periodicity of the RIS structure is much smaller than the effective wavelength of the substrate.

The EM model of the unit cell is shown in *Fig. 2(a)*, while the circuit model of the unit cell is shown in *Fig. 2(b)*. Gaps between the small patches on the ground could be modeled as a capacitor placed at a distance h (1.524 mm) from the short-circuited, dielectric-loaded transmission line. The antenna patch that is placed at a distance h from the small RIS patch can be modeled as a lumped shunt inductor parallel to the capacitor.

Circuit analyses and EM simulations were performed to investigate the effects of the RIS structure on a plane wave impinging on it, much like the analysis performed in ref. 15. For the incident plane wave, the surface impedance of the RIS is found as:

$$Z_{RIS} = j[(X_L X_C)/(X_C - X_L)] \quad (1)$$

where

$$X_L = Z_d \tan(kh) = Z_d \tan(k_0(\varepsilon_r)^{0.5} h) \quad (2)$$

$$X_C = 1/(\omega C_{RIS}) \quad (3)$$

where

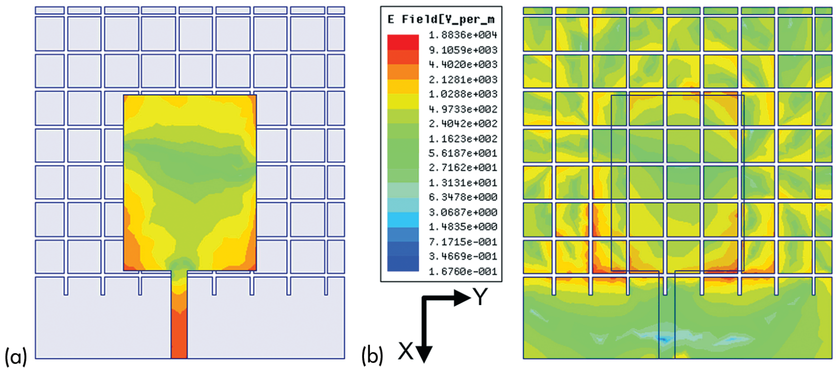

5. These simulated near-field distributions show (a) the E-field on the patch and (b) the E-field on the ground.

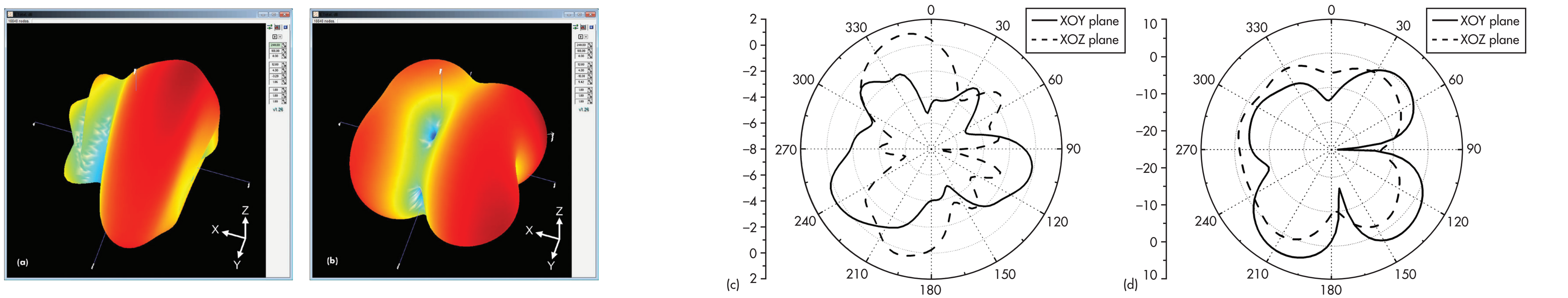

6. These plots offer far-field radiation patterns: (a) for the 3D gain pattern at 1.8 GHz, (b) the 3D gain pattern at 4.2 GHz, (c) the XOY and XOZ planes at 1.8 GHz, and (d) the XOY and XOZ planes at 4.2 GHz.

X_L and X_C are the reactances of the inductor and capacitor, respectively, shown in *Fig. 2(b)*. Detailed calculations of these two parameters can be found in ref. 15. The gap between the two adjacent small patches of the RIS structure mainly changes the capacitance value, while the dielectric permittivity and the substrate thickness mainly impact the inductor value. This combines for the resonant frequency of the RIS. The phase of the reflection coefficient of the plane wave was simulated and plotted in *Fig. 2(c)*.

The imaginary part of the surface impedance of the RIS structure was also simulated, as shown in *Fig. 2(d)*. As can be seen, the resonant frequency is located at 7.4 GHz. The RIS unit cell is inductive below the resonant frequency and capacitive above the resonant frequency. This is meaningful for the expansion of the operating frequency range of a patch antenna employing the RIS structure.

Since a patch antenna is capacitive below its resonant frequency, f_{patch}, by setting the resonant frequency of the RIS structure, f_{RIS}, higher than f_{patch}, the magnetic energy stored in the RIS structure compensates for the electrical energy stored in the near field of the patch antenna. This results in additional resonances at lower frequencies and a compact antenna size.

It should be pointed out that since the waves radiated by the patch are not plane waves and the number of RIS unit cells is finite, this analysis is just an approximation to provide physical insights into the mechanism of the RIS employed in the antenna.

Figure 3 shows the antenna's reflection coefficient. The operating bandwidth where the reflection coefficient is less than −10 dB ranges from 1.70 to 5.26 GHz. The reflection coefficient of this proposed antenna was compared with the reflection coefficient of the original antenna having the same dimensions as this proposed antenna, except that the patch and ground are intact. For the original patch antenna, *Fig. 3* shows that there is a resonance at 6.01 GHz.

Meanwhile, *Fig. 2(c)* shows that the resonant frequency of the RIS structure for the proposed antenna is located at 7.4 GHz. The inductive energy stored in the RIS below 7.4 GHz collaborates with the capacitive energy of the patch, forming the expanded operating band below 7.4 GHz. The relative bandwidth of the proposed antenna is approximately 100%, which is significantly wider than the original patch antenna. This demonstrates that the RIS structure can impact antenna resonance and extend its bandwidth.

Figure 4 shows the impedance characteristics of the antenna. There are several resonant frequencies where the imaginary part of the impedance crosses zero. The inductive energy stored in the RIS compensates for the capacitive energy of the patch antenna, thus forming several additional resonances below the resonance frequency of the original patch antenna.

This also has the effect of maintaining the real part of the impedance close to 50 Ω at these resonant frequencies, as the real part of the impedance of *Fig. 4* shows. By introducing these resonant frequencies, the operating bands of the metamaterial antenna have been extended beyond its earlier version.

Figure 5 provides simulations of the near-field distribution of the antenna. It shows the electric fields on the patch and the ground at an arbitrary frequency (3 GHz). *Figure 5(a)* shows the electric field on the patch while *Fig. 5(b)* shows the electric field on the ground.

Figure 5(a) shows that the feed energy to the antenna is effectively coupled to the patch through the microstrip line and then radiated by the edges of the patch. *Figure 5(b)* shows that the RIS structure formed by the patch and etched ground also plays a key factor in the antenna's near-field radiation, since the electric fields are distributed regularly along the edges of the strip gaps etched on the ground. This helps to form multiple radiation routes for the antenna, enhancing its radiation strength.

The far-field radiation property of the antenna was measured in terms of its radiation patterns and shown in *Fig. 6*. Two frequencies, 1.8 and 4.2 GHz, were arbitrarily chosen to verify the radiation performance of the antenna. The three-dimensional gain patterns are shown in *Fig. 6(a) and (b)* in the dB scale. The patterns of the XOY and XOZ planes at 1.8 and 4.2 GHz are also plotted in *Figs. 6(c) and 6(d)*.

As shown in *Fig. 5*, the RIS employed on the antenna affects the near-field distribution on the ground, thus making the radiation patterns of the antenna different from those of an ordinary patch antenna. At 1.8 GHz, the metamaterial-based antenna tends to radiate in the direction perpendicular to the axis of the feeding microstrip of the antenna.

The radiation pattern at 4.2 GHz also has three main lobes in the XOY plane and one main lobe in the XOZ plane. The position

7. These lots show the measured gain and efficiency for the antenna.

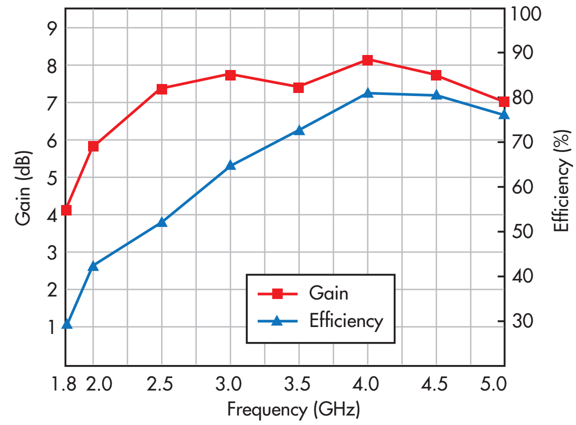

of the antenna could be adjusted so that the antenna is feasible for radiating or receiving signals in the desired direction.

Figure 7 offers the radiation gain and total efficiency of the antenna, at frequencies from 1.8 to 5.0 GHz. As can be seen, the peak gain is 7.24 dB at 4.0 GHz. The gain remains above 1.06 dB from 1.8 to 5.0 GHz. The near-field radiation from the patch, as well as that from the etched ground, help enhance the radiation gain *(Fig. 5)*. The radiation gain is in the range of 1.06 dB (at 1.8 GHz) to a maximum value of 7.24 dB (at 4.0 GHz).

From *Fig. 7*, it can be seen that the total efficiency is in the range of 54.8% (1.8 GHz) to 88.7% (4.0 GHz). This shows that the antenna can achieve efficient radiation over a wide frequency range, using a relatively simple structure in a physically compact size. mw

ACKNOWLEDGMENTS

This work was supported by the Starting Funding of Doctors of Guangdong University of Technology under Grant 405115008, the SRF for ROCS, SEM, the Innovation Project of Students of Guangdong University of Technology, and the Youth Science Funds of Guangdong University of Technology under Grant 13QNYB004.

REFERENCES

1. W.T. Li, Y.Q. Hei, W. Feng, and X.W. Shi, “Planar antenna for 3G/Bluetooth/WiMAX and UWB applications with dual band-notched characteristics,” IEEE Antennas and Wireless Propagation Letters, Vol. 11, 2012, pp. 61-64.
2. O.M. Khan, Z.U. Islam, Q.U. Islam, and F.A. Bhatti, “Multiband high-gain printed Yagi array using square spiral ring metamaterial structures for S-band applications,” IEEE Antennas and Wireless Propagation Letters, Vol. 13, 2014, pp. 1100-1103.
3. F. Bilotti, A. Alu, and L. Vegni, “Design of miniaturized metamaterial patch antennas with Mu-negative loading,” IEEE Transactions on Antennas and Propagation, Vol. 56, No. 6, 2008, pp. 1640-1647.
4. Y. Dong, H. Toyao, and T. Itoh, “Design and characterization of miniaturized patch antennas loaded with complementary split-ring resonators,” IEEE Transactions on Antennas and Propagation, Vol. 60, No. 2, 2012, pp. 772-785.
5. K. Agarwal, Nasimuddin, and A. Alphones, “RIS-based compact circularly polarized microstrip antennas,” IEEE Transactions on Antennas and Propagation, Vol. 61, No. 2, 2013, pp. 547-554.
6. Y.H. Ge, K.P. Esselle, and T.S. Bird, “The use of simple thin partially reflective surfaces with positive reflection phase gradients to design wideband, low-profile EBG resonator antennas,” IEEE Transactions on Antennas and Propagation, Vol. 60, No. 2, 2012, pp. 743-750.
7. W.Q. Cao, B.N. Zhang, A.J. Liu, D.S. Guo, T.B. Yu, and Y. Wei, “A dual-band microstrip antenna with omnidirectional circularly polarized and unidirectional linearly polarized characteristics based on metamaterial structure,” Journal of Electromagnetic Waves and Applications, Vol. 26, No. 1, 2012, pp. 274-283.
8. R.O. Ouedraogo, E.J. Rothwell, A.R. Diaz, K. Fuchi, and A. Temme, “Miniaturization of patch antennas using a metamaterial-inspired technique,” IEEE Transactions on Antennas and Propagation, Vol. 60, No. 5, 2012, pp. 2175-2182.
9. Y.H. Liu, K. Song, Y. Qi, S. Gu, and X. P. Zhao, “Investigation of circularly polarized patch antenna with chiral metamaterial,” IEEE Antennas and Wireless Propagation Letters, Vol. 12, 2013, pp. 1359-1362.
10. S. Saadat, H. Mosallaei, and E. Afshari, “Radiation-efficient 60 GHz on-chip dipole antenna realized by reactive impedance metasurface,” IET Microwaves Antennas and Propagation, Vol. 7, No. 2, 2013, pp. 98-104.
11. H.X. Xu, G.M. Wang, J.G. Liang, M.Q. Qi, and X. Gao, “Compact circularly polarized antennas combining meta-surfaces and strong space-filling meta-resonators,” IEEE Transactions on Antennas and Propagation, Vol. 61, No. 7, 2013, pp. 3442-3450.
12. L.W. Li, Y.N. Li, T.S. Yeo, J.R. Mosig, and O.J.F. Martin, “A broadband and high-gain metamaterial microstrip antenna,” Applied Physics Letters, Vol. 96, No. 16, 2010, p. 164101.
13. T. Liu, X.Y. Cao, J. Gao, Q. Yang, and W.Q. Li, “Design of miniaturized broadband and high gain metamaterial patch antenna,” Microwave and Optical Technology Letters, Vol. 53, No. 12, 2011, pp. 2858-2861.
14. H. Xiong and J.S. Hong, “A wideband endfire directional microstrip antenna with metamaterials,” IETE Journal of Research, Vol. 59, No. 2, 2013, pp. 150-155.
15. H. Mosallaei and K. Sarabandi, “Antenna miniaturization and bandwidth enhancement using a reactive impedance substrate,” IEEE Transactions on Antennas and Propagation, Vol. 52, No. 9, 2004, pp. 2403-2414.